Locally conformal method for acoustic finite-difference time-domain modeling of rigid surfaces

Julius G. Tolan and John B. Schneider

Citation: The Journal of the Acoustical Society of America **114**, 2575 (2003); doi: 10.1121/1.1616576
View online: http://dx.doi.org/10.1121/1.1616576
View Table of Contents: http://asa.scitation.org/toc/jas/114/5
Published by the Acoustical Society of America

Locally conformal method for acoustic finite-difference time-domain modeling of rigid surfaces[a)]

Julius G. Tolan[b)] and John B. Schneider[c)]
School of Electrical Engineering and Computer Science, Washington State University, Pullman, Washington 99164-2752

(Received 15 January 2001; accepted for publication 11 August 2003)

The finite-difference time-domain method is a simple but powerful numerical method for simulating full-wave acoustic propagation and scattering. However, the method can demand a large amount of computational resources. Traditionally, continuously curved boundaries are represented in a stair-step fashion and thus accurately modeling scattering from a boundary will require a finer discretization than would otherwise be necessary for modeling propagation in a homogeneous medium. However, a fine discretization might not be practical due to limited computational resources. A locally conformal technique is presented here for modeling acoustic scattering from continuously curved rigid boundaries. This technique is low cost, simple to implement, and gives better results for the same grid discretization than the traditional stair-step representation. These improvements can be traded for a coarser discretization which reduces the computational burden. The improved accuracy of this technique is demonstrated for a spherical scatterer. © *2003 Acoustical Society of America.* [DOI: 10.1121/1.1616576]

PACS numbers: 43.20.Fn, 43.30.Ft, 43.20.Px [VWS] Pages: 2575–2581

I. INTRODUCTION

The finite-difference finite-time (FDTD) method was introduced by Yee in 1966 for the purpose of modeling electromagnetic wave propagation.[1] The method is simple to implement and can readily be applied to other types of wave propagation phenomena, e.g., Refs. 2 and 3.

Modeling scattering from continuously curved boundaries with the traditional FDTD method requires a stair-step representation of those boundaries because the field update equations use material properties defined only at discrete spatial locations. When performing such modeling, using a finer discretization, i.e., reducing the spatial step size, will yield more accurate results; however, refining the grid increases the computational resource requirements. For example, when modeling a three-dimensional problem, if the grid step size is reduced by one-half, the required computer memory increases by a factor of 8 and the time required to solve the problem increases by a factor of 16. Due to limited computational resources, finer grid discretizations might not be practical and instead a coarser grid will have to be used and the resulting lower accuracy tolerated.

In this paper we introduce a locally conformal method for modeling rigid boundaries in acoustic FDTD simulations. Rigid boundaries have been used in various models including that of the human head.[4,5] An FDTD model of a rigid human head has been reported[6] where a stair-step representation was used.

The algorithm presented here uses special update equations for the pressure nodes adjacent to rigid boundaries while using regular update equations for all other nodes (including velocity nodes). The algorithm can be implemented with minimum effort, and it is found that the solution accuracy is improved significantly. Locally conformal methods for pressure-release surfaces have also been developed and can be found in the literature.[7] The locally conformal pressure-release schemes are only pertinent to the case of Dirichlet boundary conditions. Although they are similar in concept to the approach described here, they do not apply to the Neumann boundary conditions which govern rigid objects.

An alternative approach for better representing curved boundaries or boundaries not aligned with a Cartesian grid is a globally conformal technique such as presented by Botteldooren.[8] The construction of the grid in a globally conformal technique can be quite complicated. Furthermore, globally conformal techniques may not be able to use directly standard tools that have been developed for Cartesian grids (such as absorbing boundary conditions, near-field to far-field transformations, etc.). In the technique we propose this is not a concern since the technique does not distort the grid away from the surface of the scatterer. Finally, globally distorted grids have inherent numeric artifacts that are difficult to quantify *a priori* (e.g., a plane wave that propagates through a globally distorted grid representing a homogeneous medium typically will not emerge as a plane wave).

II. CONFORMAL TECHNIQUE

We begin our development with the governing differential equations in three dimensions,

$$\frac{\partial p}{\partial t} = -\rho c^2 \nabla \cdot \mathbf{v} = -\rho c^2 \left(\frac{\partial v_x}{\partial x} + \frac{\partial v_y}{\partial y} + \frac{\partial v_z}{\partial z} \right), \tag{1}$$

[a)]Presented in part at the 140th Meeting of the Acoustical Society of America.
[b)]Present address: Northrop Grumman Space Technology, 15051 Avenue of Sciences, San Diego, CA 92128.
[c)]Author to whom correspondence should be addressed; electronic mail: schneidj@eecs.wsu.edu

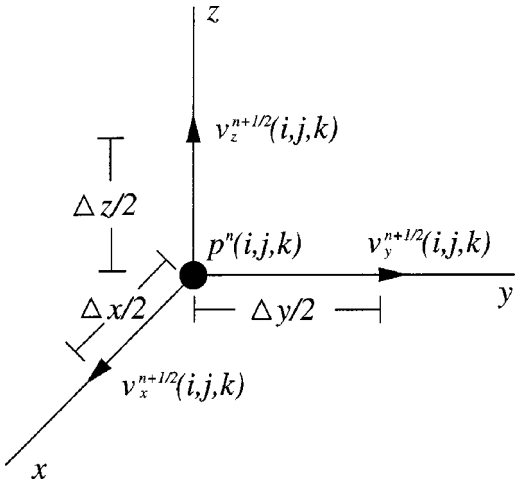

FIG. 1. Position of pressure and velocity nodes in a Cartesian grid. Different fields with the same spatial indices (i, j, k) are not collocated. For example, $v_x(i,j,k)$ and $p(i,j,k)$ are offset by a half spatial step in the x direction.

$$\frac{\partial \mathbf{v}}{\partial t} = -\frac{1}{\rho}\nabla p \rightarrow \begin{cases} \dfrac{\partial v_x}{\partial t} = -\dfrac{1}{\rho}\dfrac{\partial p}{\partial x}, \\ \dfrac{\partial v_y}{\partial t} = -\dfrac{1}{\rho}\dfrac{\partial p}{\partial y}, \\ \dfrac{\partial v_z}{\partial t} = -\dfrac{1}{\rho}\dfrac{\partial p}{\partial z}, \end{cases} \tag{2}$$

where p is the pressure, $\mathbf{v} = v_x\hat{\mathbf{a}}_x + v_y\hat{\mathbf{a}}_y + v_z\hat{\mathbf{a}}_z$ the velocity, ρ the density, and c the speed of sound. The density and speed may both be inhomogeneous.

To solve a problem using the FDTD method, we begin by replacing the derivatives with finite differences. Figure 1 shows a Cartesian grid arrangement of nodes that can be used for this replacement. The velocity and pressure nodes are known only at fixed locations in space and only at discrete times. The spatial location of the fields is indicated by the indices (i,j,k) such that $f(i,j,k)$ implies the physical location $(i\Delta x, j\Delta y, k\Delta z)$ where f is one of the fields and Δx, Δy, and Δz, are the step sizes in the x, y, and z directions, respectively. Furthermore, there is an additional offset of the fields as indicated in Fig. 1 so that each of the velocity components is offset a half spatial step from the pressure node with the same indices. (One could explicitly include these offsets in the indices, but they are dropped when implementing the algorithm in a computer. For notational convenience and to facilitate translation into code, we leave the offsets as being implied by the field component itself.) The temporal index is n. Velocity nodes are offset from pressure nodes by a half temporal step, but all velocity components are evaluated at the same instant of time, i.e., pressure nodes are defined to exist at integer multiples of the temporal step Δt while the velocity nodes v_x, v_y, and v_z, exist at times halfway between the times at which the pressures are defined. In contrast to the spatial indices, we will indicate explicitly the offset in temporal locations of the fields.

This arrangement of offset nodes allows the calculation of pressures from velocities at a previous time, and the calculation of velocities from these updated pressures. This alternating calculation is repeated for each successive time step

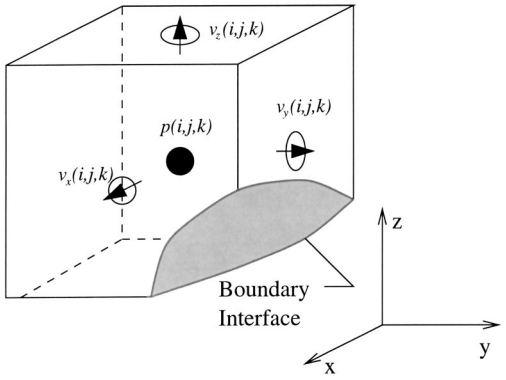

FIG. 2. Cell intersected by a rigid boundary with the portion inside the boundary removed.

as the simulation is run from an initial time to a final time. By replacing the derivatives with finite differences according to the node arrangement shown in Fig. 1, the following (traditional) update equations can be obtained from the governing differential equations (1) and (2):

$$p^{n+1}(i,j,k) = p^n(i,j,k) - \Delta t \rho c^2 \left(\frac{[v_x^{n+1/2}(i,j,k) - v_x^{n+1/2}(i-1,j,k)]}{\Delta x} + \frac{[v_y^{n+1/2}(i,j,k) - v_y^{n+1/2}(i,j-1,k)]}{\Delta y} + \frac{[v_z^{n+1/2}(i,j,k) - v_z^{n+1/2}(i,j,k-1)]}{\Delta z} \right), \tag{3}$$

$$v_x^{n+1/2}(i,j,k) = v_x^{n-1/2}(i,j,k) - \frac{\Delta t}{\rho}\left(\frac{p^n(i+1,j,k) - p^n(i,j,k)}{\Delta x} \right), \tag{4}$$

$$v_y^{n+1/2}(i,j,k) = v_y^{n-1/2}(i,j,k) - \frac{\Delta t}{\rho}\left(\frac{p^n(i,j+1,k) - p^n(i,j,k)}{\Delta y} \right), \tag{5}$$

$$v_z^{n+1/2}(i,j,k) = v_z^{n-1/2}(i,j,k) - \frac{\Delta t}{\rho}\left(\frac{p^n(i,j,k+1) - p^n(i,j,k)}{\Delta z} \right), \tag{6}$$

where the superscripts represent the temporal index, and the arguments the spatial indices. These update equations require that material properties change only at discrete locations. This implies that continuous boundaries have to be represented in a stair-step fashion.

The conformal technique presented here is similar to the one presented by Dey and Mittra for modeling perfect conductors in three-dimensional electromagnetic simulations.[9] We begin by integrating Eq. (1) over a volume V, which is bounded by a surface S, and then use the divergence theorem to obtain:

$$\frac{d}{dt}\int_V p\, dv = -\rho c^2 \int_V \nabla \cdot \mathbf{v}\, dv = -\rho c \oint_S \mathbf{v} \cdot d\mathbf{s}. \tag{7}$$

The integration can now be applied to a unit cell in the FDTD grid, centered on the pressure node at (i,j,k), which is intersected by an arbitrary rigid boundary, as shown in Fig. 2. In applying the integration, note that the normal component of velocity is zero over the rigid boundary, so the surface integral over that area is zero. Velocities are assumed constant over the portion of each face that lies outside the rigid boundary and the pressure is assumed constant throughout the cell volume which is outside the boundary. Carrying out the integration with these assumptions yields

$$\begin{aligned}\frac{dp(i,j,k)}{dt}V(i,j,k) = -\rho c^2[&A_x(i,j,k)v_x(i,j,k)\\ &-A_x(i-1,j,k)v_x(i-1,j,k)\\ &+A_y(i,j,k)v_y(i,j,k)\\ &-A_y(i,j-1,k)v_y(i,j-1,k)\\ &+A_z(i,j,k)v_z(i,j,k)\\ &-A_z(i,j,k-1)v_z(i,j,k-1)], \quad (8)\end{aligned}$$

where $V(i,j,k)$ is the cell volume outside the rigid boundary and $A_m(i,j,k)$ is the area of a cell face outside the rigid boundary, where m represents one of the surface normal directions x, y, or z. Approximating the temporal derivative with a finite difference, the following pressure update equation is obtained

$$\begin{aligned}p^{n+1}(i,j,k) = p^n(i,j,k) - \frac{\rho c^2 \Delta t}{V(i,j,k)}[&A_x(i,j,k)v_x^{n+1/2}(i,j,k)\\ &-A_x(i-1,j,k)v_x^{n+1/2}(i-1,j,k)\\ &+A_y(i,j,k)v_y^{n+1/2}(i,j,k)\\ &-A_y(i,j-1,k)v_y^{n+1/2}(i,j-1,k)\\ &+A_z(i,j,k)v_z^{n+1/2}(i,j,k)\\ &-A_z(i,j,k-1)v_z^{n+1/2}(i,j,k-1)]. \quad (9)\end{aligned}$$

This equation is used to update only the pressure in unit cells that are intersected by a rigid boundary. The velocity nodes adjacent to these pressure nodes are updated with Eqs. (4)–(6) since no special treatment is required. Furthermore, all other fields outside the rigid boundary are updated with the usual update equations Eqs. (3)–(6). If Eq. (9) is applied to a unit cell that is totally outside the rigid boundary, it can easily be shown that Eq. (9) reduces to Eq. (3).

When implementing Eq. (9) the volume and areas should be calculated before time-stepping begins. To calculate these quantities, we first need to identify all cells intersected by rigid boundaries. This can be accomplished by checking all the corners of a particular cell to see if at least one corner lies on the opposite side of a rigid boundary from the others. To increase further the processing speed, cells that are far enough from boundaries that they do not run the risk of intersecting them can be screened out with a simpler criterion based only on the location of the cell center. The more precise corner checking test can then be applied to the remaining cells.

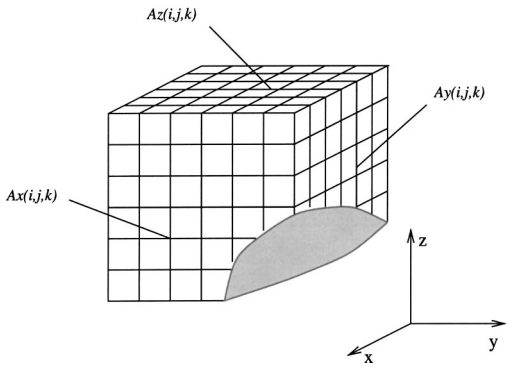

FIG. 3. A cell intersected by a rigid boundary which has been subdivided to facilitate volume and area calculations.

Once a cell is identified as being intersected by a boundary, its volume and areas can be calculated using a simple summation process. This process begins by subdividing a cell into smaller subcells, as illustrated in Fig. 3. The next step is to count all subcells that have their center outside the boundary. The total number is then used to determine the volume $V(i,j,k)$. Similarly, to find the face areas $A_m(i,j,k)$, the centers of all the squares on a particular cell face which result from the subdivision of the cell can be checked to see if they lie outside the rigid boundary. Their total number is then used to determine the areas $A_m(i,j,k)$. Note that the subdivision of cells is only done in the preprocessing phase to facilitate calculation of the geometric parameters needed in Eq. (9). The subdivision scheme described here merely requires a routine that can determine if a point is inside or outside the rigid boundary. If more detailed geometric information were needed, a different technique, such as analytic integration over the specified boundary, could be used to determine the geometric parameters. However, given the simplicity of the subdivision scheme and given a sufficiently fine level of subdivisions, it is anticipated that the subdivision approach will be preferable to the alternatives.

Stability of an FDTD simulation is another consideration that needs to be addressed. For propagation in a Cartesian grid, stability is ensured if

$$\Delta t \leqslant \frac{1}{c\sqrt{\frac{1}{\Delta x^2}+\frac{1}{\Delta y^2}+\frac{1}{\Delta z^2}}}. \quad (10)$$

For a uniform grid this reduces to, $c\Delta t/h \leqslant 1/\sqrt{3}$, where $\Delta x = \Delta y = \Delta z = h$. The dimensionless quantity $c\Delta t/h$ is the Courant number. However, when the conformal algorithm is implemented with a Courant number equal to the $1/\sqrt{3}$ limit, instability will occur for cells where the volume $V(i,j,k)$ is less then a certain minimum value $V_{\min}$ which was found empirically to be about 2% of the total volume of an undistorted cell. The instability can be removed if the cells with volume $V(i,j,k)$ less then $V_{\min}$ are treated as though they are completely inside the boundary, i.e., one resorts to stair stepping for these cells. For a Courant number of half the limit,

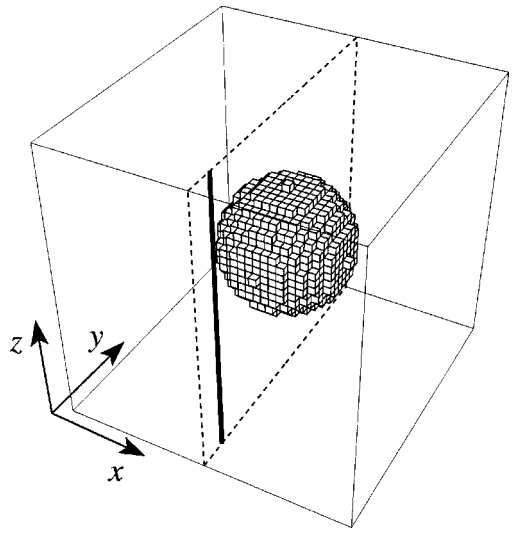

FIG. 4. Representation of the 3D computational domain used to obtain the scattered pressure from a rigid sphere. The sphere is depicted in accordance with its stair-step representation. The incident plane wave travels in the $+z$ direction and the scattered pressure is collected along the position of the heavy vertical line.

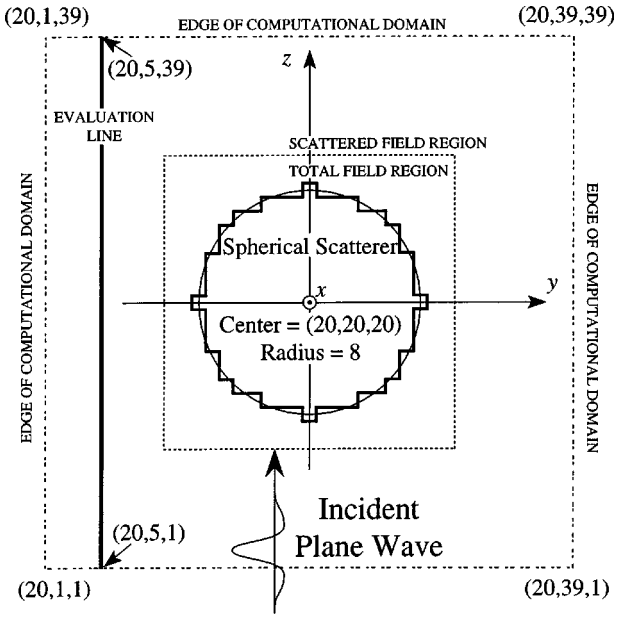

FIG. 5. Cross section of the computational domain at $x=20$. Scattered pressures are collected along the position of the heavy line.

$V_{\min}$ decreases to about 0.05% of the total volume of an undistorted cell. This yields a better representation of the boundary since one resorts to stair stepping only when 99.95% of a cell is already inside the rigid boundary; hence, only a slight error is introduced by assuming the remaining 0.05% of the cell is also within the rigid boundary.

The cost of lowering the Courant number is an increase in numeric dispersion and an increase in the number of time steps needed to propagate the field over a given distance. The increase in dispersion typically represents a small error and is more than offset with the improvement gained by the better representation of the rigid boundary. The increase in run time is inversely proportional to the reduction of the Courant number. Note that there is typically only a negligible increase in the amount of memory needed to implement the conformal technique. Hence if a computer is capable of running a simulation using a traditional staircase representation, that same simulation can be run at the same level of discretization on the same computer using the conformal technique. Reducing the Courant number by 50% and using the same level of discretization doubles the run time for the conformal technique. However, as shown in the next section, because of its increased accuracy, the conformal technique allows one to trade discretization (and accuracy) for run time. For example, if the spatial step size in the conformal technique were doubled, the simulation would run eight times faster than the traditional solution, and yet the conformal technique may still yield more accurate results.

III. RESULTS

The rigid-boundary conformal algorithm has been tested on a rigid sphere which is depicted as a staircased boundary in Fig. 4. This geometry was chosen since it permits comparison with an analytic solution. The sphere was illuminated with an incident plane wave traveling in the $+z$ direction and the scattered pressure collected over the heavy vertical line. The wave form of the incident field was chosen to be a Ricker wavelet with a peak spectral content corresponding to 20 cells per wavelength. The sphere has a radius of eight cells. The exact location of the sphere and the scattered pressure observation locations are shown in Fig. 5, which is a *yz* slice of the computational domain through the center of the sphere.

The computational domain had $39\times39\times39$ cells with an eight-cell wide perfectly matched layer (PML) surrounding it. The purpose of the PML, which is not shown in Fig. 5, is to prevent reflections from the termination of the FDTD grid.[3,10,11] A total-field/scattered-field formulation[12] was used to introduce the plane wave excitation. The simulation was run with a Courant number 50% of the limit and with a $V_{\min}$ value equal to 0.05% of the total volume of an undistorted cell. The simulation was run for 512 time steps and the scattered pressures at three different frequencies were obtained by use of a discrete Fourier transform (DFT).[12]

The FDTD results are compared with the exact analytic solution for pressures scattered from a rigid sphere of radius *a*, given by[13]

$$p(r,\theta)=\sum_{m=1}^{\infty} A_m P_m(\cos\theta) h_m(kr), \tag{11}$$

where P_m is the Legendre polynomial, h_m is the spherical Hankel function, r is the radial distance from the center of the sphere to the observation point, k is the wave number, and θ is the angle between the incident wave vector and the observation vector. The coefficients A_m are given by

$$A_m=-(2m+1)(i^m)\frac{j_m'(ka)}{h_m'(ka)}, \tag{12}$$

where the prime indicates differentiation with respect to the argument.

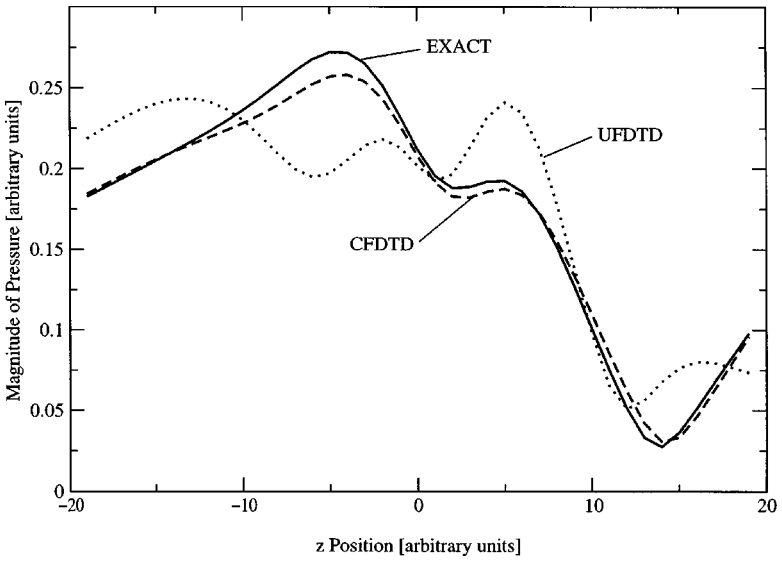

FIG. 6. Scattered pressure at 9.853 (nominally 10) points per wavelength. The independent variable is position in terms of cells where zero corresponds to the same z location as the center of the sphere.

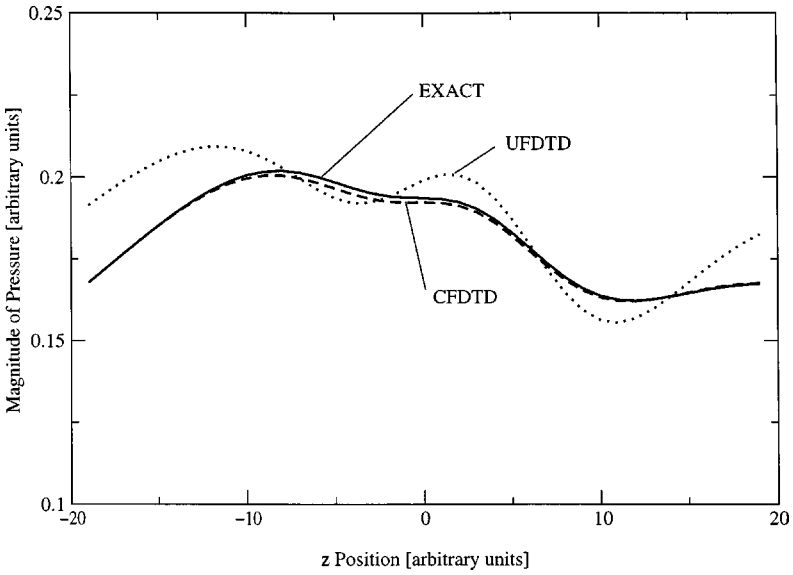

FIG. 7. Scattered pressure at 21.11 (nominally 20) points per wavelength.

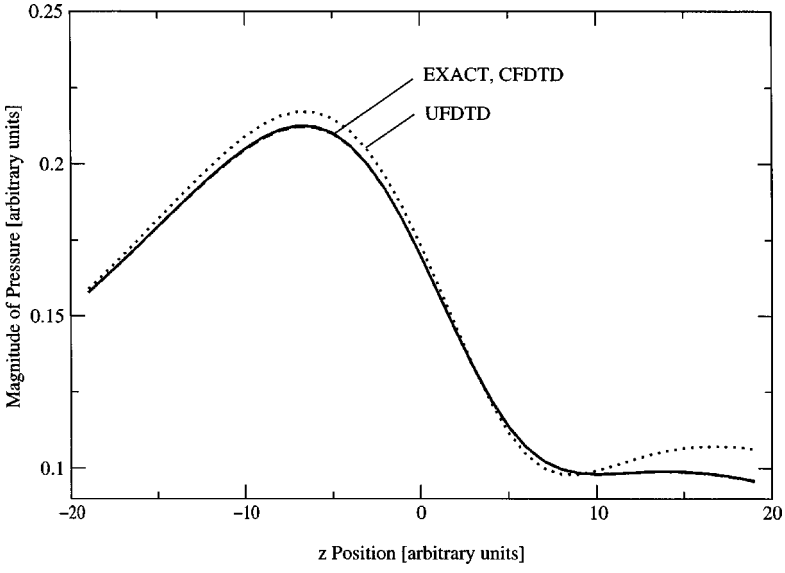

FIG. 8. Scattered pressure at 36.95 (nominally 40) points per wavelength.

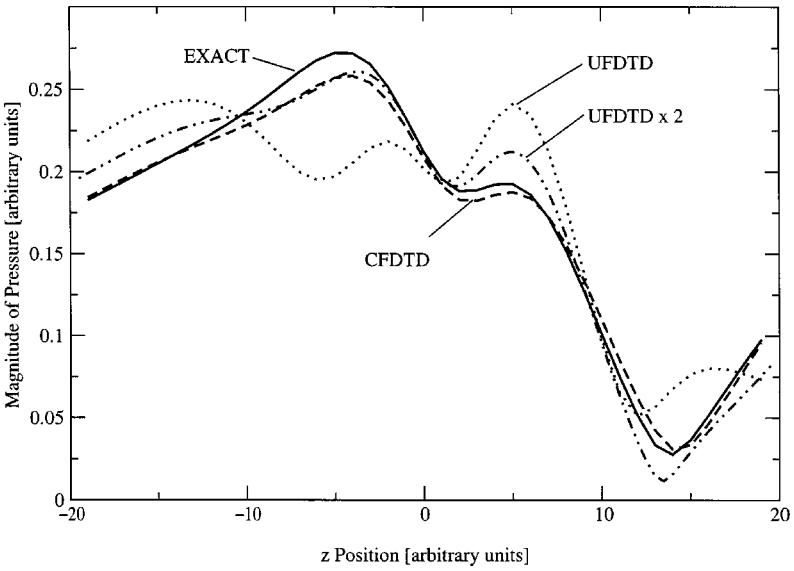

FIG. 9. Same frequency as in Fig. 6 corresponding to a *ka* of 5.026. The curve labeled "UFDTD×2" is obtained by using twice as many points per wavelength as were used to generate the previous results (i.e., by halving the spatial step size but maintaining the same geometry and *ka*).

Figures 6–8 show the scattered pressure for three different frequencies with wavelengths approximately equal to 10, 20, and 40 points per wavelength. (The actual frequencies that were obtained are dictated by the duration of the simulation and the nature of the discrete Fourier transform and correspond to 9.853, 21.11, and 36.95 points per wavelength. Nevertheless, for convenience we identify these discretizations by their approximate or "nominal" values.) Each plot shows the exact analytic result as well as the results obtained from the conformal FDTD (CFDTD) method and the traditional uniform FDTD (UFDTD) method (i.e., the stairstep approach). The pressures are normalized with respect to the incident wave. As shown in Fig. 6, at 10 points per wavelength the UFDTD method differs significantly from the exact result. The conformal method is much better but errors are still easily visible in the plot. As shown in Fig. 7, at 20 points per wavelength the UFDTD method still differs significantly from the exact solution while the CFDTD method is only slightly below the exact solution through the middle of the computational domain. As shown in Fig. 8, at 40 points per wavelength the exact and CFDTD results are nearly identical while the UFDTD result is still visibly different from the exact result. Note that these results pertain to any absolute frequency—the only important consideration is the size of the scatterer relative to a wavelength.

To illustrate further the superiority of the conformal technique, again consider the frequency and discretization shown in Fig. 6. At this frequency the scatterer has a *ka* of 5.026. We now construct a new uniform FDTD solution that halves the discretization used to obtain the previous results. Thus the sphere now has a radius of 16 cells and the computational domain is $78\times78\times78$ cells. Using this finer discretization we extract the results corresponding to a *ka* of 5.026. These results, labeled "UFDTD×2," are shown in Fig. 9 together with the previous results. By halving the discretization (and thus increasing the memory requirement by a factor of 8), the scattered field obtained using the UFDTD method has improved, but it is still not, on average, as good as the original CFDTD results. For this particular example the CFDTD method out-performs the UFDTD method even when the UFDTD method uses eight times the memory and runs eight times slower than the CFDTD method.

IV. CONCLUSION

The use of a stair-step representation of curved rigid boundaries in FDTD simulations can produce significant errors. The conformal method presented here requires modified pressure update equations only for cells adjacent to the boundary. The method is simple to implement and requires a negligible increase in memory relative to a traditional solution with the same discretization. The method does require a reduction in the Courant number to ensure stability and this can increase run-time. However, the increased accuracy of the conformal technique does offer the option of trading some accuracy (via use of a coarser discretization) for improved run time. This method was shown to produce improved results for scattered pressure from a rigid sphere and similar improvements can be expected for other geometries. Though results were not presented here, this method has been applied to other geometries which include both convex and concave surfaces.

ACKNOWLEDGMENTS

Funding for this work was provided by the Office of Naval Research, Code 321OA.

[1] K. S. Yee, "Numerical solution of initial boundary value problems involving Maxwell's equations in isotropic media," IEEE Trans. Antennas Propag. **14**, 302–307 (1966).
[2] J. Virieux, "*SH*-wave propagation in heterogeneous media: Velocity-stress finite difference method," Geophysics **49**, 1933–1942 (1984).
[3] J. G. Maloney and K. E. Cummings. "Adaptation of FDTD techniques to acoustic modeling," 11th Annual Review of Progress in Applied Computational Electromagnetics, Monterey, CA, 1995, Vol. 2, pp. 724–731.
[4] B. F. G. Katz, "Boundary element method calculation of individual head-related transfer function. I. Rigid model calculation," J. Acoust. Soc. Am. **110**, 2440–2448 (2001).
[5] B. F. G. Katz, "Boundary element method calculation of individual head-related transfer function. II. Impedance effects and comparisons to real measurements," J. Acoust. Soc. Am. **110**, 2449–2455 (2001).
[6] T. Xiao and Q. H. Liu, "Finite difference computation of head-related

transfer function for human hearing,'' J. Acoust. Soc. Am. **113**, 2434–2445 (2003).
[7] J. B. Schneider, C. L. Wagner, and R. J. Kruhlak, ''Simple conformal methods for finite-difference time-domain modeling of pressure-release surfaces,'' J. Acoust. Soc. Am. **104**, 3219–3226 (1998).
[8] D. Botteldooren, ''Acoustical finite-difference time-domain simulation in a quasi-Cartesian grid,'' J. Acoust. Soc. Am. **95**, 2313–2319 (1994).
[9] S. Dey and R. Mittra, ''A locally conformal finite-difference time-domain (FDTD) algorithm for modeling three-dimensional perfectly conducting objects,'' IEEE Microw. Guid. Wave Lett. **7**, 273–275 (1997).
[10] X. Yuan, D. Borup, J. W. Wiskin, M. Berggren, R. Eidens, and S. A. Johnson, ''Formulation and validation of Berenger's PML absorbing boundary for the FDTD simulation of acoustic scattering,'' IEEE Trans. Ultrason. Ferroelectr. Freq. Control **44**, 816–822 (1997).
[11] J.-P. Berenger, ''A perfectly matched layer for the absorption of electromagnetic waves,'' J. Comput. Phys. **114**, 185–200 (1994).
[12] A. Taflove and S. Hagness, *Computational Electrodynamics: The Finite-Difference Time-Domain Method*, 2nd ed. (Artech House, Boston, MA, 2000), pp. 356–359.
[13] P. M. Morse and H. Feshbach, *Methods of Theoretical Physics* (McGraw-Hill, New York, 1953), pp. 1483–1486.